2012

Assessment of high-enthalpy air chemistry models for hypervelocity ground-based experiments

Marat Kulakhmetov
Purdue University

Yevgeniy A. Bondar

Mikhail S. Ivanov

Alina A. Alexeenko
Purdue University - Main Campus, alexeenk@purdue.edu

Assessment of High-Enthalpy Air Chemistry Models for Hypervelocity Ground-Based Experiments

Marat Kulakhmetov[a], Yevgeniy A. Bondar[b], Mikhail S. Ivanov[b] and Alina A. Alexeenko[a]

[a]*School of Aeronautics and Astronautics, Purdue University, West Lafayette, IN 47907, USA*
[b]*Computational Aerodynamics Lab, ITAM, Novosibirsk, Russia*

Abstract. Hypersonic vehicles re-entering Earth's atmosphere with orbital velocities generate gas flows with significant thermo-chemical non-equilibrium. Detailed kinetics of chemical reactions at such conditions is still not well understood but it may affect vehicle's thermal loads, aerodynamic moments and thermal radiation. This work assesses the Total Collision Energy (TCE) and the Kuznetsov-based state specific (KSS) chemical reaction models at pressures between 1 and 50 torr and velocities between 4 and 10 km/s in order to identify best test conditions for validating the models. Hypersonic flows at such conditions can be studied at the hypervelocity impact range facilities.

Keywords: Hypersonic Aerothermodynamics, Uncertainty Quantification, Chemically Reacting Flows.
PACS: 51.10.+y, 34.50.Lf, 05.70.Ln, 07.05.Fb

INTRODUCTION

Vehicles re-entering Earth's atmosphere with orbital velocities generate flows with enthalpies in excess of 25 MJ/kg and significant thermo-chemical non-equilibrium. High fidelity thermo-chemical reaction, radiation and gas-surface interaction models are required in order to accurately predict aero-thermal loads that the re-entry vehicles experience. However, the majority of currently used hypersonic chemical reaction rates and models are based on experiments conducted at relatively low flow enthalpies and with high uncertainties [1]. The accuracy of these models, when they are extrapolated to higher temperatures, is questionable. This work investigates the feasibility of validating the Total Collision Energy (TCE) and the Kuznetsov-based state specific (KSS) direct simulation Monte Carlo (DSMC) chemical models by hypervelocity light-gas gun experiments. The reader is directed to [2] for a review of other chemical reaction models, including state-to-state kinetics, that are appropriate for DSMC applications.

The Small Particle Hypervelocity Impact Range (SPHIR) [3] is one of the hypervelocity facilities in the United States. The facility uses a light gas gun that is capable of accelerating 5-6 mg, 2 mm projectiles to velocities up to 10 km/s. The chemical composition of gasses in the test chamber can be adjusted to simulate entry into Earth's or Mars' atmospheres without facing limitations of shock tubes. The feasibility of observing the free flying SPHIR projectiles with UV-VIS spectroscopy techniques has been studied in [4]. Present work identifies test conditions required for generating distinct radiative observables. This paper first summarizes the considered chemistry models, then it presents numerical approach used to identify ideal test conditions, and finally it presents the results and conclusions.

DSMC CHEMISTRY MODELS

The total collision energy (TCE) [5] and the Kuznetsov-based State Specific (KSS) models [6] are considered in this work. For both models the discrete rotational and vibrational energies are assumed, and the rotational and vibrational levels are given by the models of nonrigid rotator and anharmonic oscillator, respectively. The TCE model assumes that the probability of two colliding molecules reacting depends only on the total energy of the

28th International Symposium on Rarefied Gas Dynamics 2012
AIP Conf. Proc. 1501, 1122-1128 (2012); doi: 10.1063/1.4769667

collision. The functional form of TCE probability of chemical reaction is chosen so that the model reproduces the Arrhenius rate equation in thermal equilibrium,

$$K_0(T) = AT^b \exp\left(-E_a / T\right), \tag{1}$$

The version of the model modified for discrete internal energies is used in the present work [7].

The KSS model can be considered a generalization of the TCE model. The vibrationaly specific chemical reaction cross sections are found numerically so that the two-temperature rate constant,

$$K\left(T,T_v\right) = Z\left(T,T_v\right)K_0\left(T\right), \tag{2}$$

is reproduced at conditions of Boltzmann distributions of translational, and rotational energies at temperature T, and vibrational energies at temperature T_v. Here, $Z(T,T_v)$ is a coupling factor given by the expression of Kuznetsov [8].

$$g(T,T_v) = \exp\left(\frac{E_v^*}{kT} - \frac{E_v^*}{kT_v}\right)\frac{\left[1-\exp(-\theta_v / T_v)\right]}{\left[1-\exp(-\theta_v / T)\right]}. \tag{3}$$

In Eq. (3), E_v^* equals to 0.7 of the dissociation energy and θ_v is the characteristic vibrational temperature. The main difference between this model and the TCE model is that it has a vibrational favoring, i.e. the vibrational energy contributes to the probability of reaction more than translational or rotational energy of the colliding molecules. This fact is illustrated in Figure 1, where the probability of the dissociation reaction,

$$N_2(n) + N_2 \rightarrow 2N + N_2, \tag{4}$$

is presented for different vibrational states, n, as a function of total collision energy (sum of translational, rotational and vibrational energy of colliding molecules.) The vibrational energy of the second molecule is not included in the KSS model. Both of the presented models are calibrated based on experimental data and they accurately capture reaction rates in equilibrium. The reaction probability in the KSS model increases as the vibration state increases, therefore excited molecules are more likely to dissociate. The probability of dissociation for TCE model does not depend on the vibrational state. The TCE model predicts higher dissociation probability at lower collision energies while the KSS model predicts higher probability at higher collision energies.

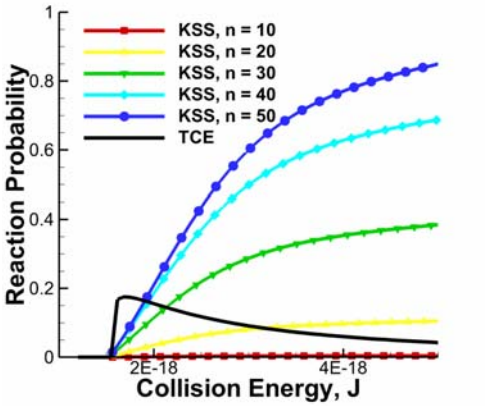

FIGURE 1. KSS and TCE reaction probabilities for N_2+N_2. Both models are calibrated based on experimental data.

The chemical kinetic mechanism that includes 19 dissociation and exchange reactions for 5 species: N, O, N2, NO, and O2; is used in this study. Recombination and ionization reactions are not considered in this work.

The two models mentioned above are applied to dissociation reactions of molecular nitrogen and molecular oxygen

$$N_2+M \rightarrow 2N+M$$
$$O_2+M \rightarrow 2O+M, \tag{5}$$

which exert the most pronounced effect on high-altitude aerothermodynamics (M stands for any component). The reaction rates for the two models are obtained from:

1. **KSS** model based on Shatalov's expression for one-temperature rate constant and reaction rate data of [9].
2. **TCE** model modified for discrete rotational and vibrational energies based on data of [10].

The other reactions are modeled in the similar manner in all cases. The TCE model modified for discrete rotational and vibrational energies of molecules is applied for:

1. NO dissociation reactions NO+M→N+O+M (reaction rate data of [10])

2. Zel'dovich reactions N2+O↔NO+N and NO+O↔O2+N (reaction rate data of Bose and Candler as presented in [11]).

NUMERICAL APPROACH

The DSMC code, SMILE [12] is used to calculate flowfields generated by a 2 mm spherical projectile traveling between 4 and 10 km through the ballistic chamber with air at pressures between 1 and 50 torr. The corresponding Knudsen numbers based on projectile diameter vary between 2×10^{-2} and 4×10^{-4}. The calculations use axisymmetric formulation with radial weights. The computational domain is presented in Fig. 2. The elastic collisions are simulated with the variable soft sphere (VSS) model and the collisions with translation-rotation and translation-vibration energy exchange are simulated with the Larsen-Borgnakke model. The size of the computational domain is kept constant for all free-stream conditions. The time step is chosen based on the mean collision time in the densest portions of the flow. Up to 100 million particles and 20 million cells are used in typical computation.

By using a 2nd order generalized polynomial chaos expansion (gPCE) with Legendre polynomials to generate response surfaces, the DSMC simulations with each chemistry model had to be run at just 9 collocation points with different values of pressure (6.522, 25.5, 44.5 torr) and projectile velocity (4.7, 7, 9.32 km/s). The translational temperature flowfields for different chamber pressures and for 7 km/s velocity are presented in Fig. 2a. With increase in pressure, the translational temperature in the shock layer and in the wake drastically decreases due to the effect of dissociation. As can be seen in the plot of response surface in Fig. 2b, this effect is more significant at higher free stream velocities.

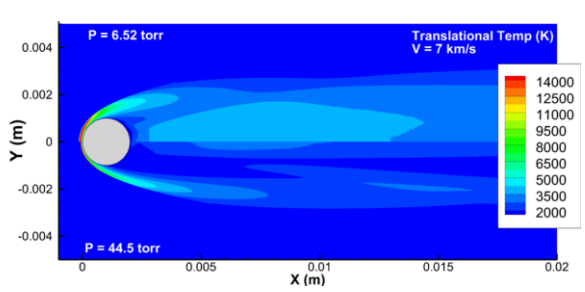

a) Flowfield translational temperature with TCE

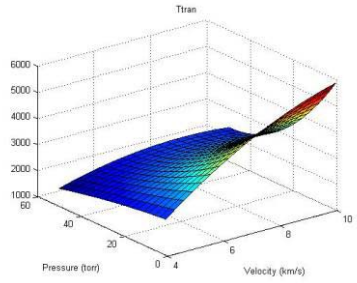

b) Translational temperature response surface in the wake, 5mm (2.5 diameters) downstream from the stagnation point

FIGURE 2. The influence of pressure on flowfield translational temperatures.

The two dimensional gPCE [13,14] is provided in Eq. (6),

$$T(x,y,\mathrm{var}) = \sum_{j=0}^{N}\sum_{i=0}^{N-j} a_{i,j}(x,y,\mathrm{var})\psi_i(V_\infty)\psi_j(P_\infty), \tag{6}$$

where x and y are spatial variables, var is the dependent flowfield variable being studied, $a_{i,j}$ are gPCE coefficients, ψ_i are Legendre polynomials of order i, and N is the order of the expansion. Because the Legendre polynomials are orthogonal, the gPCE coefficients can be obtained by multiplying Eq. (6) by another set of Legendre polynomials, taking expectation of both sides and re-arranging, as is shown in Eq. (7).

$$a_{i,j}(x,y,\mathrm{var}) = \frac{1}{<\psi_{i,j}^2>}\sum_{k=0}^{I-1}\sum_{l=0}^{I-1} Y(V_k,P_l,x,y,\mathrm{var})\psi_i(V_k)\psi_j(P_l)f_i(V_k)f_j(P_l)w_k w_l \tag{7}$$

In Eq. (7), Y is the value of the output variable, *var*, obtained from a calculation at pressure collocation point P_l, and velocity collocation point V_k, and w are Gaussian weights of Gaussian quadrature of order I. Once the gPCE coefficients are calculated, Eq. (6) can be used for all further integrations.

The response surfaces predict flow parameters based on launch conditions. In order to validate the chemistry models the projectile should be launched at conditions that would lead to greatest deviation between model predictions. These conditions are identified by fitting a normal probability distribution function to each response surface point, Eq. (8), and locating regions with minimum intersection, I, as is shown in Eq. (9). In Eq. (8), $y(M_x)$ is the prediction of property y from model M_x and σ_{exp} is the expected standard deviation in experimental data.

$$f(y \mid M_x(V_\infty, P_\infty)) = f_{norm}(y \mid \bar{y} = y(M_x), \sigma = \sigma_{\exp}) \quad . \tag{8}$$

$$I(V_\infty, P_\infty) = \int f\left(y \mid M_1(V_\infty, P_\infty)\right) * f\left(y \mid M_2(V_\infty, P_\infty)\right) dy \quad . \tag{9}$$

RESULTS AND DISCUSSION

A comparison of the flowfields of translational temperature obtained with the TCE and KSS models at the small pressure and high velocity collocation points is presented in Fig. 3a, while a comparison between N mole fractions at low pressure and intermediate velocity is presented in Fig 3b. The KSS model predicts higher temperature (about 1000 K higher) in the whole flowfield. There is also a small difference in bow shock stand-off distance (it is higher for the KSS model). The source of this difference is that the TCE model predicts a higher number of the dissociation reactions, which can be seen in Fig 3b, where the mole fractions of atomic nitrogen is about 50 % higher for TCE model. Translational temperature and N more fractions along the axis of symmetry are presented in Fig 3c and 3d, respectively. Qualitatively similar results are obtained for the other points. The mole fractions of O and NO are shown in Fig. 4 for medium and small pressure, respectively. For both of these cases TCE model predicts greater radical mole fractions.

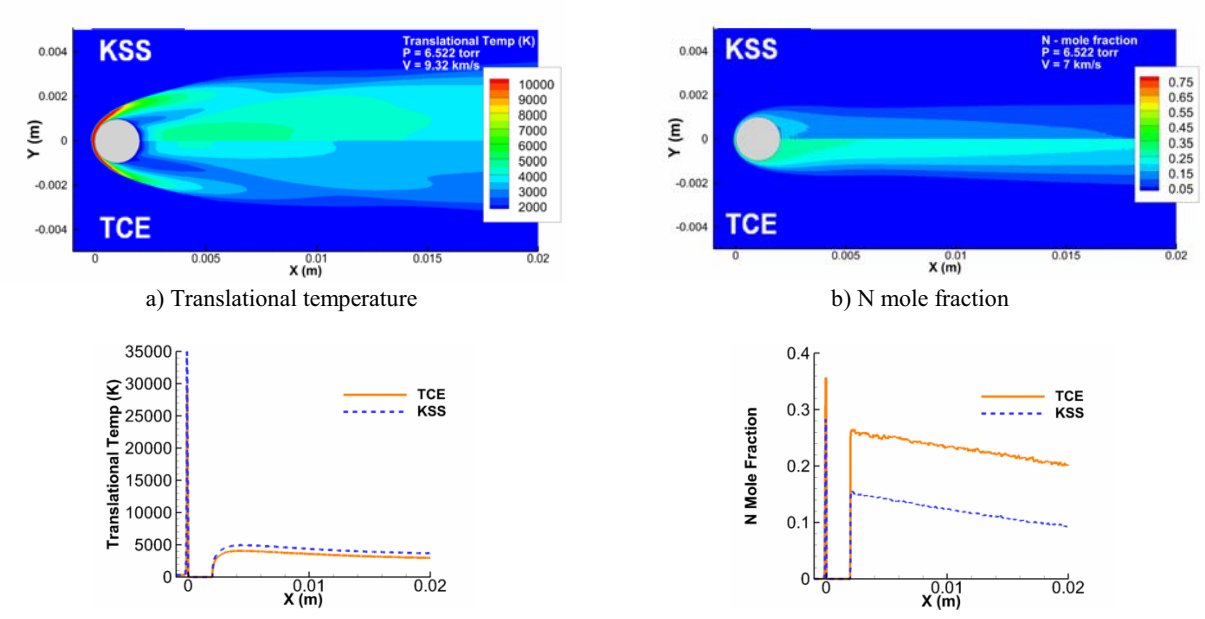

a) Translational temperature

b) N mole fraction

c) Translational temperature along the axis

d) N mole fraction along the axis

FIGURE 3. Influence of different free stream parameters and chemistry models on flowfield predictions

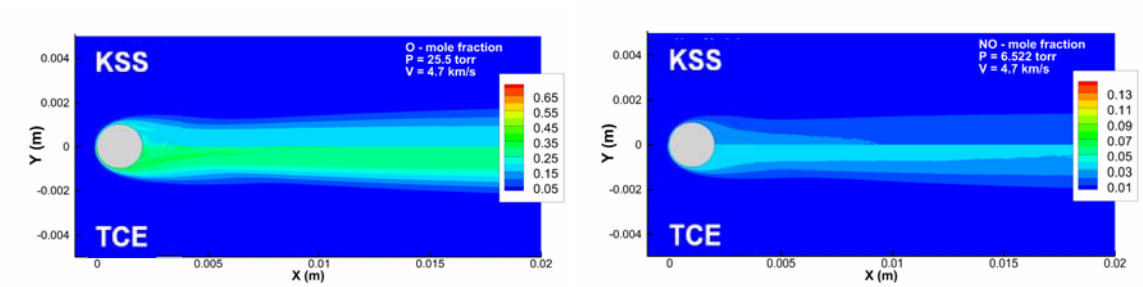

a) O mole fractions in the flowfields

b) NO mole fractions in the flowfield

FIGURE 4. Mole fractions for different free stream parameters and chemistry models.

The generalized polynomial chaos expansion is generated in all computational cells in the DSMC domain. The expansion is then used to compute model intersections based on Eq. 9. These intersections are summed for all cells and plotted in Fig. 5 for translational temperature, N, O and NO mole fractions. The lowest translational temperature intersection is found at the highest freestream velocity and lowest pressure because these conditions lead to highest collision energies and lowest equilibration rate. The lowest O an NO intersections are found at lowest velocities because both models predict almost complete O_2 and NO dissociations at higher velocities. On the other hand, since it takes more energy to dissociate N_2, lowest N intersection between the two models is found at the velocity of 8.7 km/s.

The flight conditions leading to minimum intersections of other parameters are summarized in table 1. The minimum N_2 intersection is found at conditions similar to minimum N intersection while the minimum O_2 intersection is found at a condition similar to minimum O intersection. Table 1 also provides differences between the two model predictions in the wake, 5 mm (2.5 diameters) downstream from the stagnation point. These differences are calculated directly from DSMC flowfields at two closest collocation points.

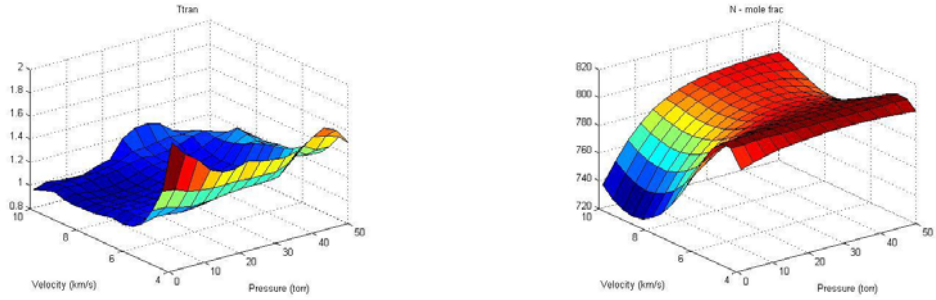

a) Translational temperature

b) N mole fraction

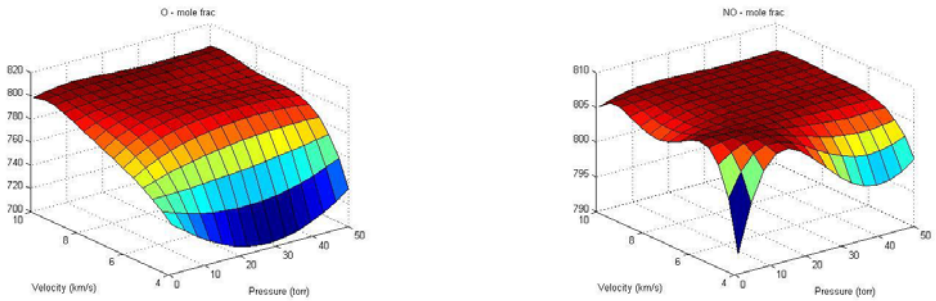

a) O mole fraction

b) NO mole fraction

FIGURE 5. Intersections computed for a range of projectile velocities and free stream pressures.

TABLE 1. Conditions for minimum model intersections

Property	Pressure (torr)	Velocity (km/s)	% Difference*
Translational Temperature	1	10	22
Rotational Temperature	1	10	16
Vibrational Temperature	50	10	30
Pressure	50	10	1
N mole fraction	1	8.7	43
O mole fraction	29	4	36
N_2 mole fraction	1	7.9	25
NO mole fraction	1	4	6.3
O_2 mole fraction	1	4	107

* % Difference is calculated in the wake, 5mm (2.5 diameters) downstream of the stagnation point based on DSMC simulations at pressure and velocity collocation points closest to the predicted minimum intersection.

CONCLUSIONS

This work is aimed at identifying test conditions that would be most suitable for validating air chemistry models. In particular, this work focuses on the Total Collision Energy (TCE) and Kuznetsov-based state specific (KSS) model predictions in the wake behind a 2 mm sphere traveling through air at velocities between 4 and 10 km/s. These test conditions could then be used to validate the two models at a hypervelocity ballistic range. The KSS model, unlike TCE, has a significant vibrational favoring and hence in the conditions of low vibrational temperature behind the shock front, it predicts fewer dissociation reactions. As the result, the KSS model predicts higher temperatures and smaller mole fractions of atomic species in the whole flowfield. The largest difference in vibrational temperatures is observed at the highest velocity and pressure. In order to observe highest differences in translational and rotational temperature, the projectile should be lunched at the lowest pressure and highest velocity. Maximum differences in NO, O_2 and O are observed at 4 km/s because higher velocities lead to almost complete dissociations. On the other hand maximum differences in N and N_2 appear at lowest pressure and at approximately 8 km/s velocity.

ACKNOWLEDGMENTS

Authors from Purdue would like to thank Sandia National Laboratory for supporting this work through the 2012 Sandia Excellence in Science and Engineering Research Fellowship.

The research carried out at ITAM was supported by the Russian Foundation for Basic Research (Grants Nos. 10-08-01203-a and 11-01-91162-a.)

REFERENCES

1. C. Park, *Nonequilibrium Hypersonic Aerothremodynamics*, Wiley, 2006, pp. 255-328
2. D. C. Wadsworth and I. J. Wysong, *Phys. Fluids* **9**, 3873-3884 (1997).
3. L. Lamberson, V. Eliasson, A. Rosakis, and M. Adams, "Mechanics of Hypervelocity Impact Induced Damage," Proceedings of the SEM Annual Conference, Albuquerque, New Mexico, 2006.
4. A. Alexeenko, M. Kulakhmetov, A. Weaver, M. Slipchenko, J. Mihaly, M. Adams, and A. Rosakis, "Feasibility of Non-Equilibrium Hypersonic Flow Measurements at the Small Particle Hypervelocity Impact Range," AIAA-2012-0596, 50th AIAA Aerospace Sciences Meeting including the New Horizons Forum and Aerospace Exposition, Nashville, Tennessee, 2012.
5. G. Bird, *Molecular Gas Dynamics and the Direct Simulation of Gas Flows*, Oxford University Press, 1994
6. Y. Bondar, and M. Ivanov, "DSMC Dissociation Model Based on Two-Temperature Chemical Rate Constant," AIAA 2007-614, 45th AIAA Aerospace Sciences Meeting, Reno, Nevada, 2007.
7. S. F. Gimelshein, N. E. Gimelshein, D. A. Levin, M. S. Ivanov, and I. J. Wysong, *Phys. Fluids* **16**, 2442-2451 (2004).
8. G. G. Chernyi, S. A. Losev, S. O. Macheret, and B. V. Potapkin, *Physical and Chemical Processes in Gas Dynamics: Cross Sections and Rate Constants for Physical and Chemical Processes*. Vol.I. Progress in Astronautics and Aeronautics, 2002.
9. L. B. Ibragimova, G. D. Smekhov, O. P. Shatalov, *Fluid Dyn.* **34**, 153-157 (1999).
10. C. Park, *J. Thermophys. Heat Tr.* **7**, 385-395 (1993).
11. C. Park, R. L. Jaffe and H. Partridge, *J. Thermophys. Heat Tr.* **15**, 76-90 (2001).

12. M. Ivanov, M. Kashkovsky, M. Gimelshein, G. Markelov, A. Alexeenko, Y. Bondar, G. Zhukova, S. Nikiforov, P. Vashenkov, "SMILE system for 2D/3D DSMC computations," Proceedings of 25th International Symposium on Rarefied Gas Dynamics, St. Petersburg, Russia, 2006, pp 21-28.
13. H. N. Najm, *Annu. Rev. Fluid Mech.* **41**, 35–52 (2009).
14. M. Kulakhmetov and A. Alexeenko, *J. Spacecraft Rockets* **49**, 461-473 (2012).